NORDIC STEEL 2024
The 15th Nordic Steel Construction Conference,
June 26–28, 2024, Luleå, Sweden

Experimental and numerical investigation of T-stub plastic resistance

Arnaud Neutelers*,[a], Adrien Corman[a], Jean-François Demonceau[a]

[a] Steel and Composite Construuction, UEE Research Unit, Liège, Belgium
arnaud.neutelers@uliege.be, adrien.corman@uliege.be, jfdemonceau@uliege.be

ABSTRACT

In structural robustness studies, column loss scenarios may be considered. Such scenarios require the structure to be calculated in its deformed configuration if a ductile response of the structure can be ensured. In case of such scenario, joint response plays a crucial role. However, nowadays, the component method for characterising joints has been essentially developed to predict (i) the elastic stiffness and (ii) the plastic resistance; in terms of ductility, only general recommendations to guarantee a sufficient ductility to perform a plastic analysis are provided. So, researches are currently being carried out on components to extend this method to predict their behaviour up to failure. However, it appears that some components such as the t-stub are still not fully mastered even in the elastic domain and their plastic resistance appears as significantly underestimated.
This article addresses the problem of predicting the plastic resistance of short unstiffened T-stubs under monotonic loading. First, a review of the current analytical models is proposed. The accuracy of these models is compared against experimental results available in the literature. Through first comparisons, it appears that assumptions made in the Eurocode mode 1 model are too conservative, leading to a significant underestimation of the plastic resistance. Therefore, a numerical model using Abaqus© is validated against the experimental tests and uses to perform a parametric analysis Allowing to realise a critical assessment of the Eurocode model assumptions.

Keywords: T-stub, Mode 1, Plastic resistance, EN1993-1-8

1 INTRODUCTION

According to the Eurocodes, in case of exceptional events, the structural stability should be ensured through an appropriate structural robustness. To achieve this goal, contributions disregarded in traditional design such as catenary effect in structural beams can be taken into account. To activate these catenary effects, large rotations should appear at the beam extremities, i.e. at the level of the beam-to-column joints and a complete mastery of their responses up to failure is therefore required. In this aim, researches were carried out at the University of Liège to extend the range of application of the Component Method (1) up to failure and, in particular, to characterise each component up to failure. Some components are already covered as the web panel in shear (2) or the column web in compression (3) while some are still under investigation.
Within the present paper, it is proposed to focus on the joint components in bending. Initially, the column flange and end-plate in bending resistances were first studied by Zoetmeijer (4). In latter, the concept of equivalent T-stub, i.e. a T-stub which plastic mechanism consists in two straight lines, one at the weld toe while the second is located at the bolt row, is defined to allow to study complex configurations into simpler ones. Many years later, Yee & Melcher (5) studied the elastic stiffness of the T-stub through a statically indetermined beam model. In 1997, Jaspart (6) made two major improvements to the models. The first one was to model the effect of the bolt head or of the nut on the connected plated through a uniform load instead of a punctual load as done in previous models. The second one was to dissociate the deformability of the bolts and of the T-stub, leading

to much simpler formulations. The so-updated model was then codified and included in the EN1993-1-8 norm and is still nowadays the model of application. However, through recent investigations conducted at the University of Liege (7), the norm was found to be too conservative for some configurations. In consequence, a rigorous experimental and numerical investigation of the most classical T-stub configuration, i.e. unstiffened back-to-back short T-stubs with one bolt row and made of mild steel welded plates, was carried out; the latter is summarised in this paper.

2 REVIEW OF THE EN1993-1-8 T-STUB RESISTANCE MODEL

The response of the idealised T-stub subjected to transverse tensile forces mainly depends of its geometrical and material properties. In particular, three main failure modes can appear as reflected in EN1993-1-8.

In case of thick plates, the failure is expected to be located in the bolts in tension either with nut stripping or thread necking. This failure mode is called Mode 3 in EN1993-1-8 and exhibits a very brittle behaviour. This collapse mode can be characterised by *Eq. 1*:

$$F_{T,3,Rd} = \sum B_{t,Rd} = \sum 0.9 f_{ub} A_s \quad (1)$$

with:

- f_{ub} : the ultimate strength of the bolt material;
- A_s : the effective area of the bolt threaded shaft.

If the bolts do not fail prior to the plate yielding, a first yielding line forms at the toe of the fillet radius or of the fillet weld between the T-stub flange and the T-stub web as illustrated in *Fig. 1.b*. Prying forces appear at the edges of the T-stub and overload the bolts. In case of thin plates, the bolts are not expected to fail and a second yielding line forms at the level of the bolt hole axis which leads to a complete plastic mechanism (see *Fig. 1.a*). This type of failure is named failure Mode 1 and can be characterised by *Eq. 2*:

$$F_{T,1,Rd} = \frac{4M_{pl,1,Rd}}{m} = \frac{4m_{pl,1,Rd}L_{eff,1}}{m} \quad (2)$$

where:

- m is the distance between the bolt hole axis and the point located at 80% of the projection of the weld thickness or fillet radius;
- $m_{pl,1,Rd}$ is the plastic resistant bending moment by unit of length of the T-stub flange;
- $L_{eff,1}$ is the effective length of the T-stub for failure Mode 1 as defined in EN1993-1-8.

An improved prediction of Mode 1 resistance is proposed by Jaspart (6) through *Eq. 3*. The latter is obtained by considering the contribution of the bolt head virtual work when computing the yield mechanism using Johanssen's theory (8):

$$F_{T,1,Rd} = \frac{(8n-2e_w)M_{pl,1,Rd}}{2mn-e_w(m+n)}. \quad (3)$$

In this equation:

- n is the distance between the bolt hole axis and the prying forces location:
  $n = \min(e\,; 1.25m)$; (4)
- $e_w = d_w/4$; (5)
- d_w is the washer diameter or the bolt head/nut diameter if there is no washer.

In the present paper, the predictions obtained using *Eq. 2* will be identified as "Method 1" while the ones obtained using *Eq. 3* as "Method 2".

An intermediate failure mode named Mode 2 can appear if the bolts fail prior to the development of the second yielding line, with account of the prying overloading. Failure Mode 2 is characterised by *Eq. 6*:

$$F_{T,2,Rd} = \frac{2M_{pl,2,Rd}+n\sum B_{t,Rd}}{m+n}. \quad (6)$$

Finally, for a specific T-stub, the failure mode that occurs is the one with the minimum resistance:

$$F_{T,Rd} = \min(F_{T,1,Rd}; F_{T,2,Rd}; F_{T,3,Rd}). \quad (7)$$

It should be mentioned that these formulae *Eqs. 1-7* are commonly accepted and widely used. Indeed, more complex models (6,9-11) aiming to predict the full behaviour of T-stub up to failure are using those formulations to characterise the latter plastic resistance.

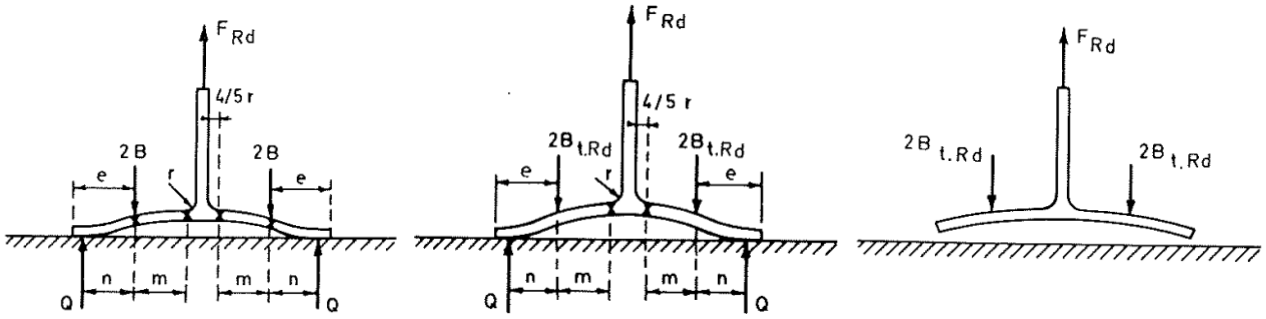

a) b) c)

Fig. 1. a) Mode 1; b) Mode 2; c) Mode 3*(6)*

3 EXPERIMENTAL DATA

A database of well-documented experimental tests on 15 specimens, within the scope of this study, was built through a literature review. Both actual geometrical and mechanical properties of the specimens are summarized in *Table 1*. Based on these properties, the above-described model can be applied for each specimen to predict their plastic resistance. The obtained results are reflected in *Table 2.* In addition, a graphical representation of the comparison between the experimental results and the analytical predictions is provided in *Fig. 2* for T-10-16-100 specimen from *Table 1-2.*

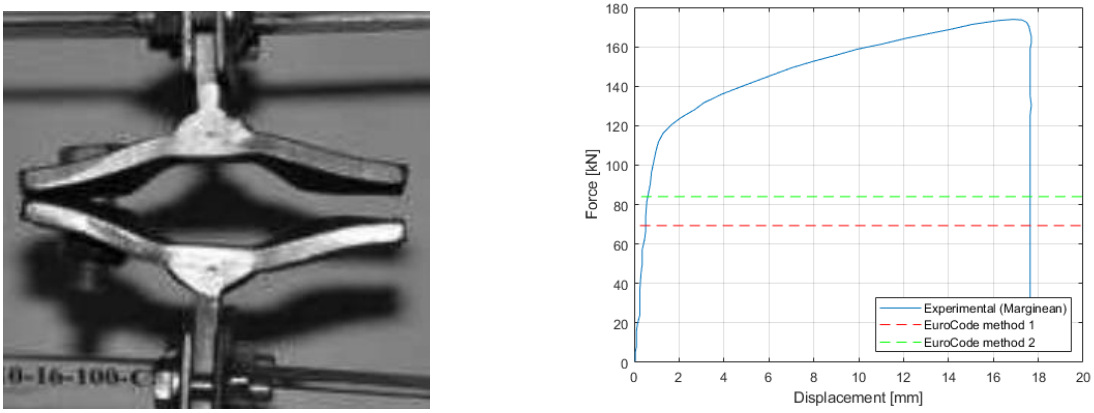

a) b)

Fig. 2. a) T10-16-100 tested specimen (12); b) experimental and analytical results for one T-stub

Based on the results of *Table 2*, some observations can be made:

- For Mode 1, the plastic resistance computed by the model, using Method 1 or Method 2, greatly underestimates the actual one. However, Method 2 is seen as more accurate than Method 1.
- Failure Mode 2 are accurately predicted.

From these observations, it is clear that the models proposed for failure Mode 1 have to be improved through a better identification and understandings of the physical phenomena influencing this failure mode. This will be done through numerical studies as reflected in the next sections.

Table 1. Geometrical and mechanical properties of the experimental tests

Author	Specimen	t_w (mm)	t_f (mm)	m (mm)	e (mm)	a_w (mm)	L (mm)	d_b (mm)	f_y (MPa)	$f_{u,b}$ (MPa)
(12,13)	T-10-16-100	10	9.6	37	30	7	90	16	310	1080
(12,13)	T-10-16-120	10	9.7	47	30	7	90	16	310	1080
(12,13)	T-10-16-140	10	9.7	57	30	7	90	16	310	1080
(12,13)	T-12-16-100	10	11.8	37	30	7	90	16	305	1080
(12,13)	T-12-16-120	10	11.8	47	30	7	90	16	305	1080
(12,13)	T-12-16-140	10	11.8	57	30	7	90	16	305	1080
(12,13)	T-15-16-100	10	15	37	30	7	90	16	275	1080
(12,13)	T-15-16-120	10	15	47	30	7	90	16	275	1080
(12,13)	T-15-16-140	10	15	57	30	7	90	16	275	1080
(12,13)	T-18-16-120	10	18	47	30	7	90	16	420	1080
(12,13)	T-18-16-140	10	18	57	30	7	90	16	420	1080
(14)	TST-17.5a-18	9.5	17.5	47.2	50	9	120	18	261	820
(14)	TST-11.5a-18	9.5	11.5	47.2	50	9	120	18	274	820
(14)	TST-11.5b-18	9.5	11.5	47.2	50	9	120	18	338	820
(14)	TST-11.5b-20	9.5	11.5	47.2	50	9	120	20	338	836

t_w: web thickness; t_f: flange thickness; a_w: weld throat thickness; L: T-stub length; d_b: bolt diameter; f_y: plate yield strength

Table 2. EN1993-1-8 model

Author	Specimen	Experimental		Method 1			Method 2		
		Mode	F_y (kN)	Mode	F_y (kN)	Rel. error (%)	Mode	F_y (kN)	Rel. error (%)
(12,13)	T-10-16-100	1	119.9	1	69.3	-42.2	1	84	-29.9
(12,13)	T-10-16-120	1	87.15	1	55.8	-36	1	65.7	-24.6
(12,13)	T-10-16-140	1	77.2	1	46	-40.4	1	53.3	-31
(12,13)	T-12-16-100	1	136.45	1	103.1	-24.5	1	124.9	-8.5
(12,13)	T-12-16-120	1	118.5	1	81.2	-31.5	1	95.7	-19.2
(12,13)	T-12-16-140	1	98	1	67	-31.7	1	77.6	-20.9
(12,13)	T-15-16-100	2	179.1	1	150.2	-16.1	2	178	-0.6
(12,13)	T-15-16-120	1	162.1	1	118.3	-27	1	139.4	-14
(12,13)	T-15-16-140	1	138	1	97.6	-29.3	1	113	-18.1
(12,13)	T-18-16-120	2	200	2	198.3	-0.9	2	198.3	-0.9
(12,13)	T-18-16-140	2	180	2	175.5	-2.5	2	175.5	-2.5
(14)	TST-17.5a-18	2	200	2	195.1	-2.5	2	195.1	-2.5
(14)	TST-11.5a-18	1	152.8	1	92.1	-39.7	1	107.5	-29.7
(14)	TST-11.5b-18	1	169	1	113.6	-32.8	1	132.6	-21.6
(14)	TST-11.5b-20	1	181	1	113.6	-37.2	1	133.9	-26
					MEAN:	-26.3		MEAN:	-16.7

4 NUMERICAL MODELLING

4.1 Modelling of T-stub material law

In the reported experimental results, some coupon test curves were provided. The latter were numerically simulated to derive the numerical material laws, including damage.

Regarding the plastic domain, the engineering stress-strain were converted into true stress- true strain with *Eqs. 8,9:*

$$\varepsilon_{true} = \ln(1 + \varepsilon_{eng}) \quad (8)$$

$$\sigma_{true} = \sigma_{eng}(1 + \varepsilon_{eng}) \quad (9)$$

These equations remains correct until the onset of necking is attained. After this point, the post-necking response is modelled considering *Eq. 10* proposed by Ling (15). This formula consists in a weighted combination of a linear and exponential formulation:

$$\sigma_{pl,true,damaged} = W\left(A\varepsilon_{pl,true} + b\right) + (1 - W)(K\varepsilon_{pl,true}^{N}) \quad (10)$$

with :

- A, the true stress at the onset of necking;
- N, the true strain at the onset of necking;
- $b = A(1 - N)$; (11)
- $K = A/N^{N}$; (12)
- W, the weighted coefficient to be determined though comparison to coupon test results.

Then, as a stopping criterion, damage is implemented in the model as growing voids, i.e. as a porosity. This dimensionless damage index variable can be formulated with *Eq. 13*:

$$D = 1 - \frac{\sigma_{pl,true,damaged}}{\sigma_{pl,true}} \quad (13)$$

Notice that damage increases up to a certain point. Once this critical damage is attained, rupture occurs and leads to a complete loss of the bearing capacity. The damage at which failure appears is unknown and must be determined by trials-and-errors, comparing the numerical results to the coupon test results.

The so-derived parameters can be consulted in *Table 3*. A mesh sensitivity analysis was also carried out to determine that the most suited element size for the coupon test simulation is 2 (mm) C3D8. In addition to that, a damage initiation criterion has to be defined. Thus, the stress state of the material has to be evaluated accounting for triaxiality through *Eq. 14*:

$$\theta = \frac{\frac{1}{3}(\sigma_{xx} + \sigma_{yy} + \sigma_{zz})}{\sigma_{mises}} \quad (14)$$

with:

- σ_{ii}, the principal stress in direction *i*;
- σ_{mises}, the Von Mises equivalent stress.

For simple stress state such as the one appearing in coupon tests, *Eq 11* becomes $\theta = 1/3$ (uni-axial stress). For more complicated stress states, a criteria is proposed by Pavlović in (16,17). It expresses as *Eq. 15*:

$$\varepsilon_{pl,true,damaged} = \alpha e^{-\beta\theta} \quad (15)$$

where :

- $\varepsilon_{pl,true,damaged}$ is the equivalent plastic strain at damage initiation;
- β is a dimensionless material parameter assumed here equal to 1.5;
- θ is the stress triaxiality;
- α is a dimensionless parameter to be determined in uniaxial tension test.

Table 3. Material laws calibrated parameters

Element	A (MPa)	N (-)	W (-)	D_{cr} (-)
web	678.47	0.187	-1.5	0.28
flange	517.54	0.2328	-0.3	0.3
M16 10.9	1,148.23	0.0112	0	0.38

For the coupon test simulation, the loading was applied through an imposed deformation with an imposed velocity of 0.1 (mm/s) in a dynamic implicit procedure until failure is reached. The density and Young modulus are respectively assumed to be 0.00785 (T/mm^3) and 210,000 (MPa). *Fig. 3.* illustrates that the force-displacement curve obtained numerically approximates satisfactorily the experimental data. A slight overestimation of the initial stiffness can be noticed. However, this error

can be neglected since the test setup stiffness is unaccounted in the model. A summary of all the parameters to be determined by trials-and-errors is proposed in *Table 3.* Similar procedure is applied to the other coupon tests.

4.2 Modelling of the bolts

Regarding the bolts, although tests were performed on the bolts, the stress-strain curves of the bolt material were not provided. However, D'Aniello performed tension tests on M16 10.9 bolt grade (18,19). In his papers, he proved that the standard deviation of the ultimate stress and strain is negligible. In consequence, the model of the bolt is based on those results. D'Aniello also pointed out that there exist two types of bolts on the European market: HR and HV bolts (18,19), but corresponding to different failure modes. Indeed, while the former fails due to necking in the threaded shaft, the latter is expected to undergo thread stripping and nut slipping. In the modelled specimens, the bolts are HR. From this perspective, the threaded shaft is modelled as a cylinder. In addition to that, the head, the shaft and the nut constituting the bolt are modelled as one unique element. Since the failure is expected to occur in the threaded part, the nut-shaft interaction can be disregarded. The implemented geometry is the nominal one found in the standards (20). The definition of the material law is done using the procedure described hereabove, simulating the bolt in Abaqus and comparing the numerical prediction to the experimental results from bolt tensile tests. The loading in the numerical simulation is applied through imposed displacement with an imposed velocity of 0.1 (mm/s) on the internal head face. All the other degrees of freedom of the head are blocked. The nut is considered as clamped on its internal face. All the parameters to be determined can be consulted in *Table 3*. On *Fig. 3*, it can be seen that both ultimate displacement and strength are well assessed. Similarly to the coupon tests, the initial stiffness is slightly overestimated. However, as for the plates, the error made is due to the setup stiffness not taken into account and can be considered as negligible. Thus, it can be concluded that the law implemented for the bolt is sufficiently accurate.

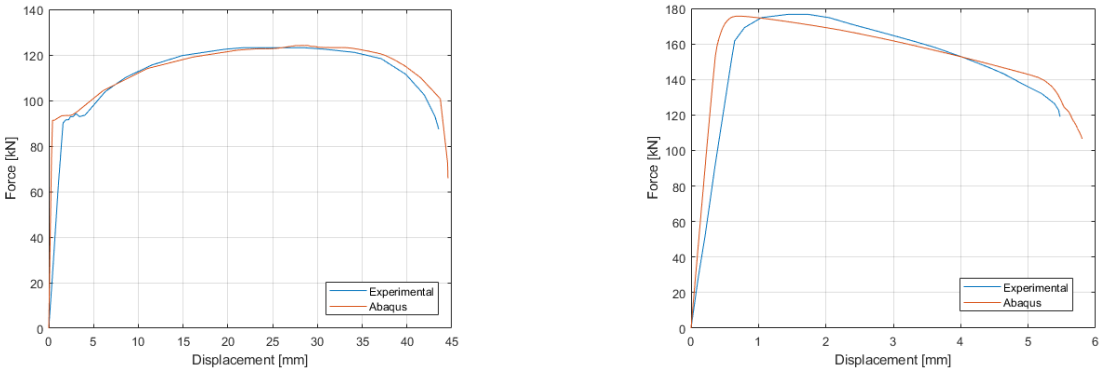

Fig. 3. a) Coupon test validation; b) Bolt coupon validation

4.3 Validation of the T-stub modelling

The actual geometric properties used to model the T-stubs can be found in *Table 1*. Regarding the bolts, the nominal geometry proposed in the standard (20) is used. To model the interaction between elements, a contact law is defined in Abaqus©. The normal contact is chosen as "hard" to prevent any overlapping while a friction coefficient equal to 0.2 is used to characterise the tangential contact. The loading, as for the previous models, is applied through an imposed displacement with a velocity of 0.1 (mm/s). This boundary condition is imposed on the free end of the web of the upper T-stub. All the other degrees of freedom at this extremity are blocked. Regarding the second T-stub, the free edge of its web is clamped. A mesh sensitivity analysis was conducted and 2 (mm) size C3D8 block elements were used. Implicit dynamic analyses were conducted. Results of the described procedure are presented on *Fig. 4.* The comparison between the Abaqus© results and the

experimental ones shows good correspondences which allows the use of the modelling procedure for a parametric analysis.

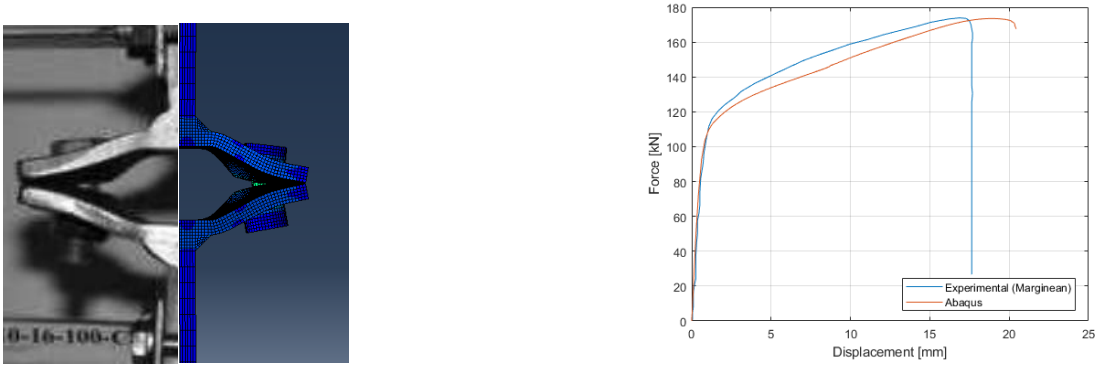

a) b)

Fig. 4. a) T10-16-100 visual validation (12); b) Graphical validation

5 PARAMETRIC STUDY

To perform the parametric study, some modifications are made to the model used for the validation process:

- the actual material law are replaced by elastic – perfectly plastic curves;
- the actual material and geometrical properties are replaced by nominal ones;
- the T-stubs are 70 (mm) length to ensure a two lines plastic mechanism.

The aim of the parametric study is to investigate a wide range of configurations to perform a critical review of the assumptions made within the EN1993-1-8 model. To do so, dimensionless parameters and their variation ranges were defined as follows:

- t_f /C ∈ [0.1 ; 0.2 ; 0.3] estimates the flange flexibility with C, the distance between the bolt axis and the weld toe;
- t_f /d_b ∈ [0.6 ; 0.7 ; 0.8 ; 0.9] indicates how close to a failure Mode 2 the specimen is;
- e/C ∈ [0.5 ; 0.8 ; 1] gives indications on the effect of the prying forces. Notice that for all specimens n = e according to *Eq 4*.

The specimen name should read T-d_b- t_f /C- t_f /d_b-- e/C.

5.1 Study of the position of the plastic hinges

The first assumption that can be investigated is the assumed position of the hinges. It can be seen on *Fig. 5* that the positions of both hinges are not corresponding to the ones assumed in the EN1993-1-8 model. Similar observation can be made for each specimen. For the first hinge, it can be observed that its location is at the weld toe or even further while it is assumed to be at 80% of the projection of the weld thickness in EN1993-1-8 model. On the other hand, the second hinge is not localised at the bolt axis but exhibits an offset towards the web.

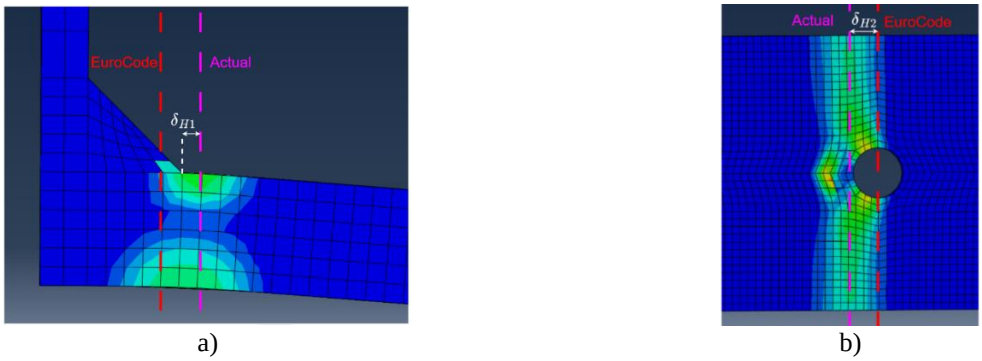

a) b)

Fig. 5. a) Plastic hinge at the weld toe ; b) Plastic hinge at the bolt hole

5.2 Study of the stress distribution under the bolt head

Through the numerical results, the stress distribution under the bolt head can be investigated. This can be done by looking the contact pressures in Abaqus© which are illustrated on *Fig. 6.* It can be observed that the uniform distribution assumed in EN1993-1-8 is not observed

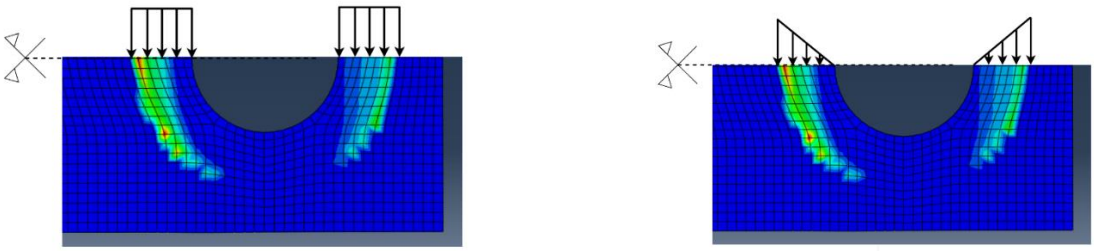

a) b)

Fig. 6. a) uniform distribution; b) Triangular distribution

Indeed, the T-stub deformation induces flexion in the bolts as suggested by the asymmetry of the stress distribution. Another consequence is that stress concentration occurs at the washer edges. From this perspective, a uniform distribution does not make sense. A triangular distribution seems more suitable to idealise the contact pressure between the T-stub flange and the washer.

5.3 Study of the position of the prying forces

A conclusion drawn from the e/C parameter is that the location of the prying forces is not adequately assumed in the EN1993-1-8 model. Indeed, as it can be seen in *Fig. 7*, all the force-displacement curves are not affected by the variation of the distance between the T-stub flange edge and the bolt while EN1993-1-8 model reflects an influence of this distance on the T-stub resistance to account for a variation of the location of the prying forces, as reflected by the red and blue horizontal lines in *Fig 7* showing the minimum and maximum resistances computed with EN1993-1-8 for the investigated T-stubs.

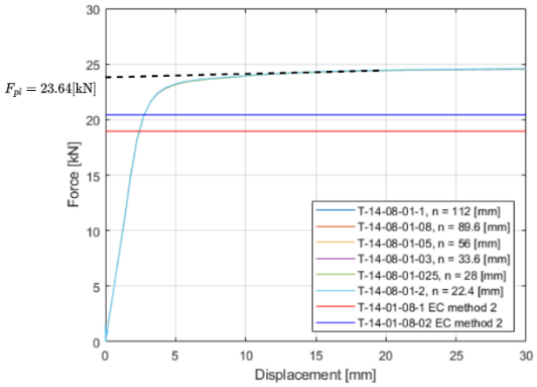

Fig. 7. Prying forces study

Fig. 8 shows the contact pressures distribution between the flanges for the two extreme cases. For the longest one, i.e.T-14-08-01-1, it can be seen that all the contact pressures are localised near the bolt hole and vanishes past a certain distance. In this case, the prying forces are assumed to apply at the flange edge while, if they were rigorously integrated, their location would be much closer to the hole. For the shortest specimen, i.e. specimen T-14-08-01-02, assuming the prying forces at the flange edge is a good approximation of the true integrative process. In fact, due to the flange flexibility, the bolts clamp the plates leading to the prying forces of all the T-stubs lying at the same location close to the bolts, which explains why all the curves of *Fig. 7* are identical. This observation reflects that a boundary is missing in the EN1993-1-8 formula for the localisation of the prying force, see *Eq. 4*.

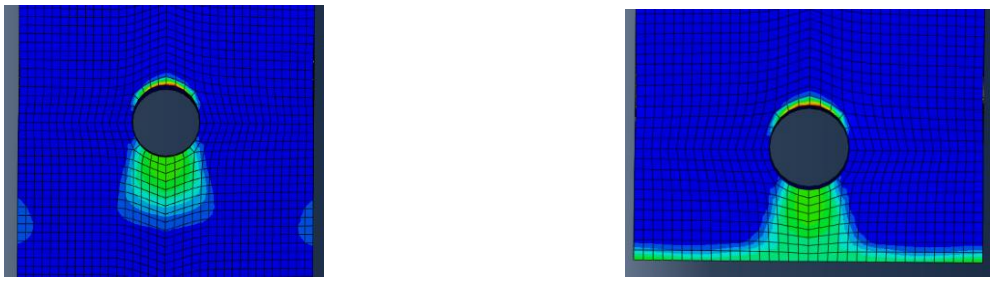

a) b)

Fig. 8. Contact pressure at the bottom face a) T-14-08-01-1; b) T-14-08-01-02

5.4 Study of the plastic mechanism

Finally, it should be pointed out that, although the length of the specimens was fixed to 70 (mm) to ensure a two lines pattern according to EN1993-1-8, some of the modelled T-stubs do not exhibit such a yield line pattern. Indeed, some have a pattern composed of two straight lines, as expected (see *Fig. 9.a*), while some show an interaction between the yield lines (see *Fig. 9.b*), the yield line at the level of the bolts exhibiting a curved part and meeting the straight yield line at the level of the weld toe.

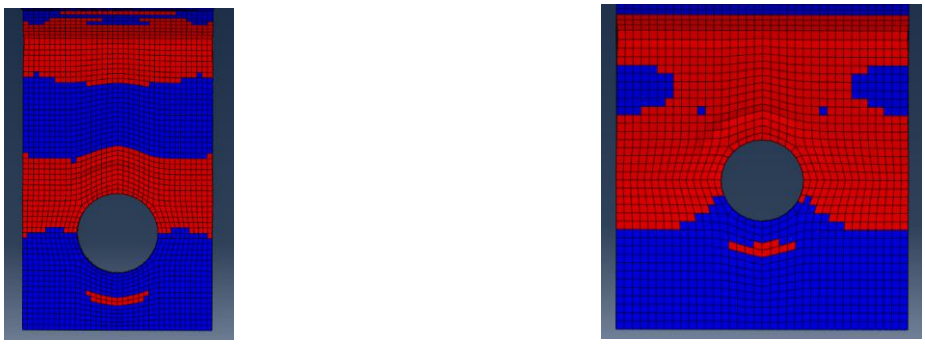

a) b)

Fig. 9. a) Two lines pattern; b) New pattern

6 CONCLUSIONS

In this paper, the assumptions behind the EN1993-1-8 model for the prediction of the plastic resistance of a T-stub failure Mode 1 were reviewed in depth, leading to the following conclusions:

- the plastic hinges are inadequately located. Indeed, according to the numerical study, the first one is located at the tip of the weld toe or even further while the second one exhibits an offset from the bolt axis towards the web;
- the stress distribution under the bolt head assumed as uniform in the EN1993-1-8 model is in fact closer to a triangular distribution;
- the prying forces were also proved to be misplaced;
- Even if the specimen length was fixed at 70 (mm) to ensure that all the T-stubs are short ones with a yield line pattern made of two straight lines, some tests showed another unaccounted yield line pattern.

The over conservativeness of the EN1993-1-8 norm highlighted in section 3, when compared to experimental evidence, can be explained by all the above listed conclusions. An ongoing research conducted at Liege University aims at improving the model prediction through a better implementation of the above-mentioned observation; some first results could be presented during the Nordic Steel 2024 conference.

REFERENCES

1. **CEN, E. N. 1-8.** *Eurocode 3: Design of Steel Structures–Part 1–8: Design of Joints.* Brussels : European committee for standardization,, 2005.
2. **CORMAN, Adrien.** *Characterization of the Full Non-Linear Behaviour up to Failure of the Sheared Panel Zone under Monotonic Loading Conditions.* Liège : University of Liège, 2022.
3. *Characterization of unstiffened column webs in transverse compression in steel beam-to-column joints.* **JASPART, Jean-Pierre, CORMAN, Adrien, et DEMONCEAU, Jean-François.** [éd.] Elsevier. 2022, Thin-Walled Structures, Vol. 180.
4. **ZOETEMEIJER, P. A.** *design method for the tension side of statically loaded, bolted beam-to-column connections.* s.l. : HERON, 20 (1), 1974, 1974.
5. *Moment-rotation curves for bolted connections.* **YEE, Yoke Leong & MELCHERS, Robert E.** no. 3, 1986, Journal of Structural Engineering, Vol. 112, pp. 615-635.
6. **NEUTELERS, Arnaud.** *Improvement of the mechanical model for mode 1 T-stub plastic strength.* Liège : s.n., 2023.
7. **JASPART, Jean-Pierre.** *Contributions to recent advances in the field of steel joints. Column bases and further configurations for beam-to-column joints and column bases.* Liège : s.n., 1997.
8. **JOHANSEN, K. W.** *Yield-line theory.* s.l. : Cement and Concrete Association , 1962.
9. *Ultimate behavior of bolted T-stubs. I: Theoretical model.* **PILUSO, Vincenzo, FAELLA, Ciro, et RIZZANO, Gianvittorio.** no 6, 2001, Journal of structural engineering, Vol. 127, pp. 686-693.
10. *Ultimate behaviour of bolted T-stubs under large displacements: A mechanical model.* **FRANCAVILLA, Antonella B., LATOUR, Massimo, et RIZZANO, Gianvittorio.** [ed.] Elsevier. 2022, Journal of Constructional Steel Research, Vol. 195.
11. *Mechanical model for the full range behaviour of bolted T-stubs.* **LYU, Jiafeng, YAN, Shen, HE, Shubin, et al.** [ed.] Elsevier. 2023, Journal of Constructional Steel Research, Vol. 200.
12. **MĂRGINEAN, Ioan Mircea.** *Robustness of moment steel frames under column loss scenarios.* s.l. : Timişoara: Editura Politehnica, 2017.
13. **ANWAR, Ghazanfar Ali.** *Ultimate deformation and resistance capacity of bolted T-Stub connections under different loading conditions.* s.l. : České vysoké učení technické v Praze, 2017.
14. *Full-range behaviour of T-stubs with various yield line patterns.* **ZHAO, Xianzhong, HE, Shubin, et YAN, Shen.** [ed.] Elsevier. 2021, Journal of Constructional Steel Research, Vol. 186.
15. *Uniaxial true stress-strain after necking.* **LING, Yun, et al.** no 1, 1996, AMP Journal of technology, Vol. 5, pp. 37-48.
16. *Connections in towers for wind converters, part I: Evaluation of down-scaled experiments.* **PAVLOVIĆ, Marko, HEISTERMANN, Christine, VELJKOVIĆ, Milan, & al.** [ed.] Elsevier. 2015, Journal of Constructional Steel Research, Vol. 115, pp. 445-457.
17. *Bolted shear connectors vs. headed studs behaviour in push-out tests.* **PAVLOVIĆ, Marko, MARKOVIĆ, Zlatko, VELJKOVIĆ, Milan, & al.** [ed.] Elsevier. 2013, Journal of Constructional Steel Research, Vol. 88, pp. 164-149.
18. *Monotonic and cyclic inelastic tensile response of European preloadable gr10. 9 bolt assemblies.* **D'ANIELLO, Mario, CASSIANO, David, & LANDOLFO, Raffaele.** [ed.] Elsevier. 2016, Journal of Constructional Steel Research, Vol. 124, pp. 77-90.
19. *Simplified criteria for finite element modelling of European preloadable bolts.* **D'ANIELLO, Mario, CASSIANO, David, & LANDOLFO, Raffaele.** no 6, 2017, Steel Compos. Struct, Vol. 24, pp. 643-658.
20. **STANDARD, BRITISH.** *High-strength structural bolting assemblies for preloading.* 2005.